Energy 78 (2014) 205–211

Contents lists available at ScienceDirect

Energy

journal homepage: www.elsevier.com/locate/energy

Numerical study of primary steam superheating effects on steam ejector flow and its pumping performance

Xiaodong Wang [a, *], Jingliang Dong [a, b], Ao Li [a], Hongjian Lei [a], Jiyuan Tu [b]

[a] School of Mechanical Engineering & Automation, Northeastern University, Shenyang 110819, PR China
[b] School of Aerospace, Mechanical and Manufacturing Engineering, RMIT University, Victoria 3083, Australia

ARTICLE INFO

Article history:
Received 25 February 2014
Received in revised form
15 July 2014
Accepted 1 October 2014
Available online 31 October 2014

Keywords:
Steam ejector
CFD
Wet steam modeling
Superheat degree
Pumping performance

ABSTRACT

The effects of primary steam superheating on steam condensation in nozzle and the performance of steam ejector were investigated using CFD (computational fluid dynamics) method. Using a wet steam model being proposed in our previous study, simulations based on the primary steam with five superheated levels were performed, and the results demonstrate the superheating operation of the primary steam weakens the spontaneous condensation intensity and postpones its occurrence within the nozzle vicinity. Due to the droplets nucleation refinement for the condensation of superheated steam, the mixing process between the primary and the secondary fluids is improved. Consequently, a higher entrainment ratio is achieved. However, the superheating operation may not exceed 20 K, as its contribution on entrainment ratio improvement is not as significant as 0 K–20 K superheating, and too much superheating will requires more energy as input, which is not a practical solution to further improve the steam ejector pumping performance.

1. Introduction

Steam ejector is widely used in chemistry, petroleum, metallurgy, refrigeration, and food industry to generate a vacuum environment for special purposes. A typical steam ejector includes four parts as shown in Fig. 1a: Laval nozzle, mixing chamber, throat and diffuser [1]. Simplified pressure and velocity distributions along the centerline of the steam ejector are depicted by Fig. 1b. First, the primary fluid, which is steam with high pressure (0.3–1.6 MPa) is accelerated to supersonic speed through the converging-diverging Laval nozzle. Then, a low pressure region is established downstream of the nozzle outlet. Driving by the pressure difference, the secondary fluid is entrained into the mixing chamber and accelerated to supersonic speed by the primary fluid. After a mixing process involving energy and momentum exchange between these two types of fluid, a normal shock wave occurs in the throat, and the velocity of the mixing fluid suddenly drops down to a subsonic level. Finally, the mixed fluid is exhausted to the next stage by the diffuser.

Entrainment ratio E_m is a widely accepted indicator to assess the pumping performance of a steam ejector, and it equals to the ratio of mass flow rate between the secondary fluid and the primary fluid. Huang et al. [2] investigated the entrainment ratio variation regarding on different operating back pressure values, and they divided the ejector operating status into three modes (Fig. 2): critical mode, subcritical mode and malfunction. When the back pressure P_b is below the critical back pressure P_b^*, the secondary flow is choked in the mixing chamber, and the entrainment ratio E_m remains constant. However, once P_b is higher than P_b^*, the secondary flow becomes unchoked, and E_m begins to decrease rapidly. When P_b is greater than the reversing back pressure P_b^r, the high back pressure jeopardizes the ejector entrainment process, leading to a flow reverse in the mixing chamber. Therefore, the steam ejector should be operated within the critical mode to maintain a steady pumping performance. As a result, accurate prediction of E_m variation regarding on different back pressure settings and the determination of the critical pressure P_b^* play critical roles in theoretical analysis and engineering applications.

Due to the transonic flow nature, the complicated mixing flow in the steam ejector is difficult to be described by classical mathematical methods [2,3]. Alternatively, computational fluid dynamics (CFD) is a good choice as a research tool to investigate and predict the internal flow behavior for steam ejectors. Although steam ejectors have been extensively studied using different numerical approaches for decades, majority of them were based on the ideal gas assumption [4–9], while influences induced by the spontaneous condensation were not taken into account. This

* Corresponding author. Tel.: +86 24 8368 7618; fax: +86 24 8368 0459.
E-mail address: xdwang@mail.neu.edu.cn (X. Wang).

http://dx.doi.org/10.1016/j.energy.2014.10.004
0360-5442/

Nomenclature

B, C	virial coefficients (m^3/kg, m^6/kg^2)
C_p, C_{p0}	isobaric heat capacity, standard state heat capacity (J/(kg K))
E_m	entrainment ratio
h, h_0	specific enthalpy, standard state enthalpy (J/kg)
h_v	vapor specific enthalpy (J/kg)
I	nucleation rate (1/s)
K_B	Boltzmann constant (J/(mol K))
k	turbulent kinetic energy (m^2/s^2),
M	molecular mass (kg)
P	pressure (Pa)
P_b	back pressure (Pa)
M	molecular mass (kg)
P	pressure (Pa)
P_b^*	critical back pressure (Pa)
P_b^r	reversing back pressure (Pa)
q_c	evaporation coefficient
R	gas-law constant (J/(mol k))
$\bar{r}$	droplet average radius (m)
r^*	critical droplet radius (m)
S	super saturation ratio
s, s_0	specific entropy, standard state entropy (J/(kg mol K))
T	thermal temperature (K)
T_0	droplet temperature (K)
t	time (s)
u	velocity (m/s)
V_d	average droplet volume (m^3)
α_v	volume fraction
β	mass fraction
γ	specific heat capacities ratio
Γ	mass generation rate (kg/s)
ε	turbulent energy dissipation rate (m^2/s^3)
η	droplet number density ($1/m^3$)
θ	non-isothermal correction factor
μ, μ_t	dynamic viscosity, turbulent viscosity (Pa s)
ν	kinetic viscosity (m^2/s),
ρ, ρ_l, ρ_v	mixture density, liquid density, vapor density (kg/m^3)
σ	droplet surface tension (N/m)

simplification may contribute to some prediction uncertainties for the determination of the entrainment ratio and the critical pressure.

As a critical part of a steam ejector, the nozzle plays a key role in the acceleration of the primary fluid and the entrainment of the secondary fluid. Thus, the associated fluid thermodynamics characteristics occurring within the nozzle are theoretically examined (Fig. 3). Along with the acceleration of the primary fluid, the saturated assumed primary fluid expands from its stagnation pressure level A to its suction pressure level B along the isentropic expansion line AC, and intersects with the isobar line CB at point C. However, the real expansion process may follows line AC' when taking the nozzle efficiency and fraction loss into consideration. It should be noted that either of the steam status at point C or C′ is in its super-saturation state as the dryness value of these two points are below one. As the current steam pressure is fairly above its saturation pressure which is determined by its current temperature. In such a circumstance, a spontaneous condensation will occur, and our previous work [10] demonstrated its existence when the supersonic flow passes through the nozzle using a wet steam modeling approach, and the wet steam model also gave a close predication of E_m [11, 12].

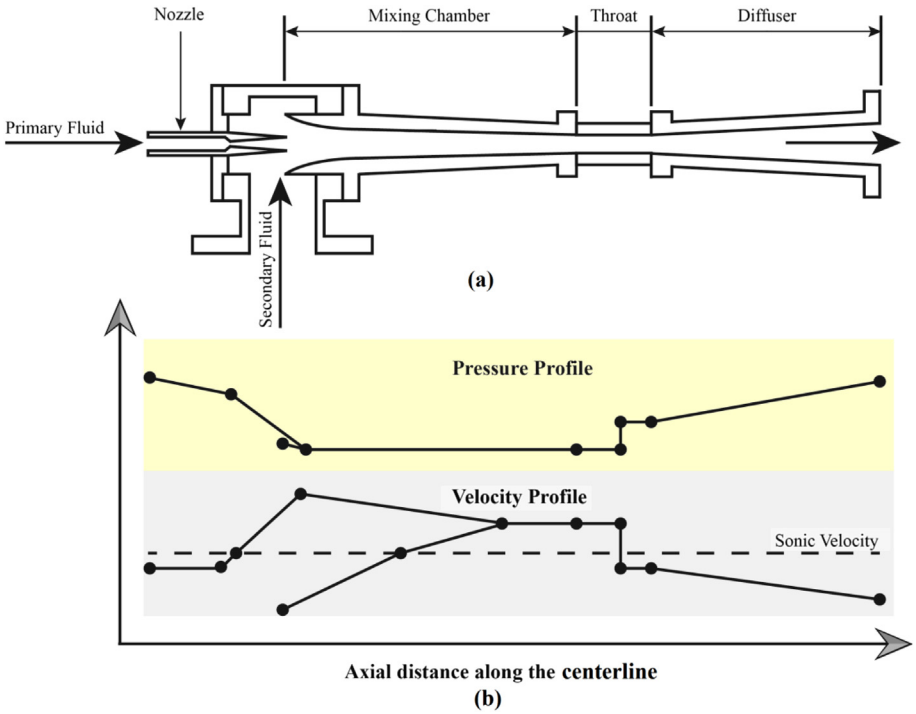

Fig. 1. Schematic diagram of a steam ejector: (a) geometry configuration (b) axial pressure and velocity profiles along the centerline.

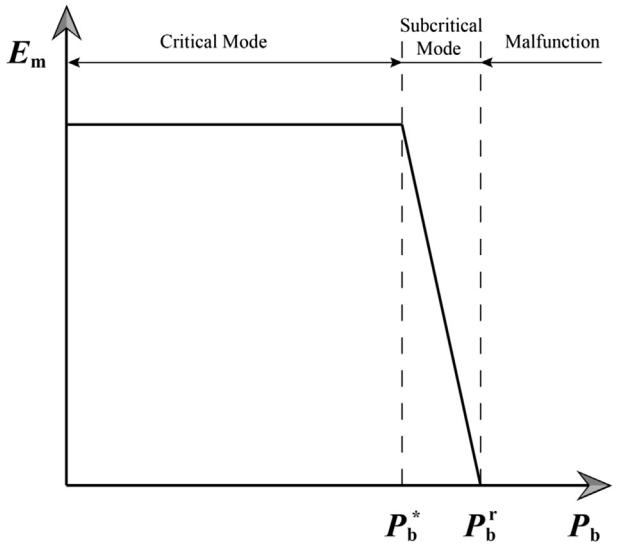

Fig. 2. Typical performance curve for a steam ejector with respect to different back pressure.

As a well-known approach to reduce mechanical damage to reciprocating engine or turbine, superheated steam in these applications shows its ability to release tremendous quantities of internal energy yet remain above the condensation temperature of water vapor at the pressures at which reaction turbines and reciprocating piston engines operate. Chunnanond and Aphornratana [1] investigated the effect of primary steam superheating experimentally, and they found only limited improvement on the ejector entrainment performance can be generated. Ludwing [13] recommended a few degrees of superheating (2.8–8.3 °C) from practical points of view, but if superheated steam is to be used, its effect must be considered in the ejector design.

Combining with the wet steam simulation approach, numerical simulations considering different primary steam superheating conditions were conducted to address the superheating effect on steam ejector flow, and its contribution on ejector entrainment ratio.

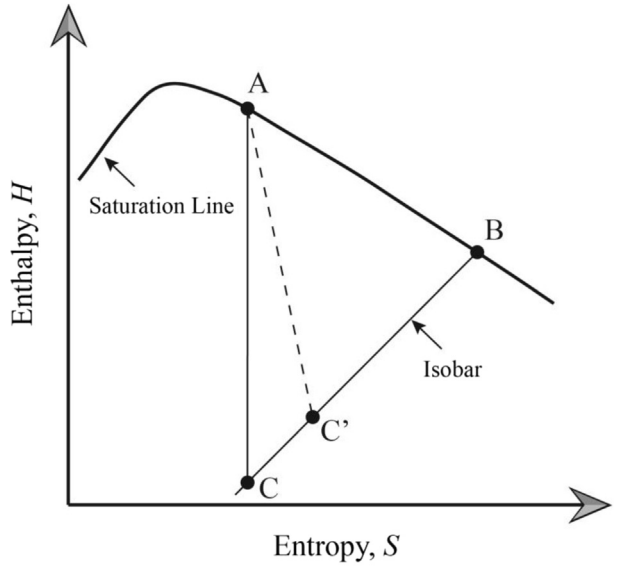

Fig. 3. Enthalpy–entropy diagram of the primary steam expansion.

2. Mathematical models of wet steam flow

The flow behaviour of the primary fluid in the nozzle was described by the Eulerian–Eulerian two-fluid model. The mass and heat transfer between vapor phase and liquid phase during condensation process, two addition transport equations of the liquid-phase mass-fraction, and the liquid-droplets number density were introduced in this model to close the two-phase continuity, momentum and energy governing equations. Several assumptions were preset in the present model as follows:

(1) The velocity slip between the droplets and gaseous-phase is negligible;
(2) As the mass fraction of the condensed phase is small, the interactions between droplets are neglected;
(3) Since droplet sizes are very small, the volume of the condensed phase and the thermal capacity are negligible.

2.1. Liquid-phase mass-fraction transport equation

The first addition transport equation governing the mass fraction of the condensed liquid phase [14] can be written as below:

$$\frac{\partial(\beta\rho)}{\partial t}+\nabla\cdot\left(\rho\beta\vec{u}\right)=\Gamma \tag{1}$$

where Γ is the mass generation rate due to condensation and evaporation, which is correlated to the nucleation rate I (the number of new droplets per unit volume per second) and the growth/demise of these droplets [14]:

$$\Gamma=\frac{4}{3}\pi\rho_l I r^{*3}+4\pi\rho_l\eta\bar{r}^2\frac{\partial\bar{r}}{\partial t} \tag{2}$$

The nucleation rate [15] can be written in this form:

$$I=\frac{q_c}{(1+\theta)}\left(\frac{\rho_v^2}{\rho_l}\right)\sqrt{\frac{2\sigma}{M^3\pi}}\exp\left(-\frac{4\pi\cdot r^{*2}\sigma}{3K_B T}\right) \tag{3}$$

here, θ is a non-isothermal correction factor [15,16] and it is given by:

$$\theta=\frac{2(\gamma-1)}{(\gamma+1)}\left(\frac{h_v}{RT}\right)\left(\frac{h_v}{RT}-0.5\right) \tag{4}$$

The wet steam density can be determined by the vapor density ρ_v and the liquid phase mass fraction β:

$$\rho=\frac{\rho_v}{(1-\beta)} \tag{5}$$

The critical droplet radius r^*, above which the droplet will grow and below which the droplet will evaporate [16], is given by:

$$r^*=\frac{2\sigma}{\rho_l RT\ln S} \tag{6}$$

The size of droplets is affected by two mechanisms: the transfer of mass from the vapor to the droplets, and the transfer of heat from the droplets to the vapor in the form of latent heat [14]. It can be written as below:

$$\frac{\partial \bar{r}}{\partial t} = \frac{P}{h_v \rho_l \sqrt{2\pi RT}} \cdot \frac{\gamma + 1}{2\gamma} C_p (T_0 - T) \tag{7}$$

2.2. Droplet number density transport equation

The droplet number density η that is defined as the number of droplets per unit volume can be expressed as:

$$\eta = \frac{\beta}{(1-\beta) V_d (\rho_l / \rho_v)} \tag{8}$$

where V_d is the average droplet volume, which is defined as: $V_d = 4/3\pi \cdot \bar{r}^3$.

The number density of the droplets transport equation obtained from Ref. [14] is described as:

$$\frac{\partial(\rho\eta)}{\partial t} + \nabla \cdot \left(\rho \eta \vec{u}\right) = \rho \mathrm{I} \tag{9}$$

2.3. State equation of wet steam

The wet steam equation of state which relates the pressure to vapor density and temperature [15] is given by:

$$P = \rho_v RT \left(1 + B\rho_v + C\rho_v^2\right) \tag{10}$$

here, B and C are the second and third Virial coefficients respectively, and are functions of temperature.

The wet steam isobaric specific heat capacity C_p, specific enthalpy h, specific entropy s, are given by Eqs. (11)–(13) [16]:

$$C_p = C_{p0}(T) + R\left(\left((1-\alpha_v T)\left(B - T\frac{dB}{dT}\right) - T^2\frac{d^2B}{dT^2}\right)\rho_v + \left((1-2\alpha_v T)C + \alpha_v T^2 \frac{dC}{dT} - T^2 \frac{d^2C}{dT^2}\Big/2\right)\rho_v^2\right) \tag{11}$$

$$h = h_0(T) + RT\left(\left(B - T\frac{dB}{dT}\right)\rho_v + \left(C - T\frac{dC}{dt}\Big/2\right)\rho_v^2\right) \tag{12}$$

$$s = s_0(T) + R\left(\ln \rho_v + \left(B + T\frac{dB}{dT}\right)\rho_v + \left(C + T\frac{dC}{dT}\Big/2\right)\rho_v^2\right) \tag{13}$$

where C_{p0}, h_0, s_0 are the standard state isobaric specific heat capacity, enthalpy, entropy.

The wet steam dynamic viscosity and thermal conductivity are functions of steam temperature and were referred from Ref. [14].

2.4. Turbulence model

The *realizable* k–ε turbulence model relies on the Boussinesq hypothesis [17] is used in present study, which is based on an eddy viscosity assumption, and the Reynolds stress tensor comes from equation averaging to be proportional to the mean deformation rate tensor:

$$-\rho \overline{u_i'} \overline{u_j'} = \mu_t \left(\partial u_i / \partial x_j + \partial u_j / \partial x_i\right) - 2/3(\rho k + \mu_t \delta u_i / \delta x_i)\delta_{ij}$$

The advantage of this approach is the relatively low computational cost associated with the determination of the turbulent viscosity, and suitable for industrial applications. The *realizable* k–ε model can be described as [18]:

$$\partial(\rho k)/\partial t + \partial\left(\rho k u_j\right)/\partial x_j = \partial\left(\left(\mu + \mu_t/\sigma_k\right)\partial k/\partial x_j\right)/\partial x_j + G_k + G_b - \rho\varepsilon - Y_M + S_k \tag{14}$$

$$\partial(\rho\varepsilon)/\partial t + \partial\left(\rho\varepsilon u_j\right)/\partial x_j = \partial\left(\left(\mu + \mu_t/\sigma_\varepsilon\right)\partial\varepsilon/\partial x_j\right)/\partial x_j + \rho C_1 S_\varepsilon - \rho C_2 \varepsilon^2 \Big/ \left(k + \sqrt{\nu\varepsilon}\right) + C_{1\varepsilon}\varepsilon/k C_{3\varepsilon} G_b + S_\varepsilon \tag{15}$$

where G_k, G_b and Y_M are the generation of turbulence kinetic energy and the contribution of the fluctuating dilatation respectively. S_k, S_ε are user-defined source terms. $C_1 = \max(0.43, \eta_1/\eta_1 + 5), \eta_1 = S_1 \cdot k/\varepsilon$, $S_1 = \sqrt{2 S_{ij} S_{ij}}$. $C_{1\varepsilon}$, C_2 are the model constants, and $C_{1\varepsilon} = 1.44$, $C_2 = 1.9$. σ_k, σ_ε are the turbulent Prandtl numbers for k and ε, and $\sigma_k = 1.0$, $\sigma_\varepsilon = 1.2$.

3. Numerical simulation settings

The geometrical parameters of the studied steam ejector proposing by Sriveerakul et al. [19] are summarized by Table 1. In order to reduce computational expenses and improve simulation efficiency, a two-dimensional axisymmetrical geometry was used in this study to represent the three-dimensional fluid domain [20].

The fluid domain was first meshed into quadrilateral elements, and then the mesh results were imported into ANSYS-Fluent (ANSYS, Inc. Pennsylvania, United States). Prior performing numerical simulations, mesh independence study was conducted using three levels of grid size, the coarse level with 9654 elements, the medium level with 55,025 elements and the fine level with 134,528 elements. Based on the comparison of axial Mach number profiles for these three mesh configurations, the Mach number profile yield by the medium mesh shows a closer agreement with the fine mesh than the coarse mesh (maximum Mach number difference less than 10%) [11]. Therefore, the medium mesh level was chosen as a mesh bench mark for all simulations throughout this study. In addition, mesh adaptation (Fig. 4a and c) and near wall refinement (Fig. 4b and d) were implemented at regions where experiencing rapid velocity gradient to better capture internal flow patterns. Pressure inlet and pressure outlet were used for numerical simulation, the turbulent kinetic energy and turbulent energy dissipation rate of inlet flow were 1 and 1, and the temperature and pressure of inlet flow are shown in Table 2.

The convection terms were discretized with second-order upwind scheme, and a central difference discretization method was used to discretize the diffusion terms. Then, the discretized system was solved by the Gauss Seidel method by choosing the coupled-

Table 1
Geometrical parameters of the steam ejector [19].

Geometrical parameters	Value
Diameter of nozzle inlet section	7.75 mm
Diameter of nozzle outlet section	8 mm
Diameter of nozzle throat	2 mm
Expand angle of nozzle	10°
Length of nozzle	60 mm
Nozzle exit position	0 mm
Diameter of mixing chamber inlet section	24 mm
Diameter of throat	19 mm
Length of mixing chamber	130 mm
Length of throat	95 mm
Length of diffuser	180 mm

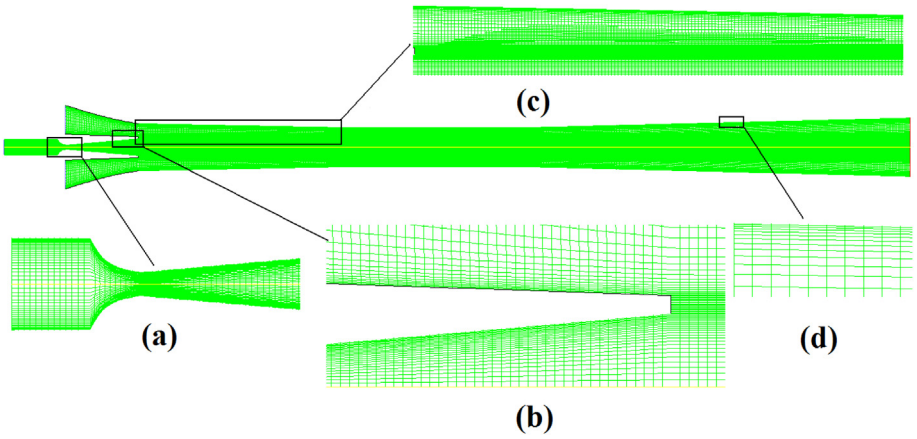

Fig. 4. The structural mesh results of the computational domain.

implicit solver. Enhanced wall treatment was used to describe the flow behaviour at the near-wall region [21]. The convergence criterion for the relative residual of all dependent variables was set to 1×10^{-6} and the mass imbalance value was set as 1×10^{-7} to ensure iteration convergence.

4. Results and discussion

4.1. Verification of numerical model

The numerical simulation accuracy was first validated against the experimental study conducted by Bakhtan and Mohammadi Tochai [22]. Since this experimental work is using different nozzle and boundary conditions, relevant geometry parameters and pressure conditions are listed in Tables 3 and 4. As shown in Fig. 5, the experimental data shows a 5,000 Pa pressure increase occurring downstream of the nozzle throat ($x = 4$ cm) due to the presence of spontaneous condensation, and the simulation results yielded from the wet steam model also presents a pressure increase. However, the occurrence location is brought forward to $x = 3$ cm, and the intensity also decreased from 5,000 Pa to 3,000 Pa. On the contrary, the numerical results predicted by ideal gas model cannot reflect this phenomenon at all. Therefore, the wet steam modeling approach can predict the spontaneous condensation with a reasonably good accuracy while the ideal gas modeling approach could not capture this at all.

Using the boundary conditions being provided in Table 2, the entrainment ratio (E_m) profile with respect to different back pressure settings was analyzed and plotted in Fig. 6. It is found that the numerical simulation results based on the wet steam model provided a much more closer prediction of E_m. For the critical mode, a E_m of 0.42 is predicted using the wet steam modeling approach, which is well agreed with the experimental E_m value 0.45 [19] with a deviation of 6.67%. However, the E_m value predicted by the ideal gas model is 0.36, which diverges from the experimental value with a deviation of 20%. Furthermore, the critical pressure P_b^* yielded by the wet steam model is around 4600 Pa, which also shows a superior agreement with the experimental value (4700 Pa), and the pressure deviation is 2.13%. However, the ideal gas model captures the P_b^* at 4400 Pa with an under prediction of 300 Pa. The pressure deviation is increased to 6.38%.

Therefore, the spontaneous condensation need to be taken into account for steam ejector simulation, as it can further improve the entrainment ratio and critical back pressure prediction accuracy comparing with the simulation neglecting this phenomenon. To investigate the superheating effects on the spontaneous

Table 2
Inlet flow conditions of the steam ejector [19].

Working fluid	Temperature (K)	Pressure (Pa)
Primary fluid	403	270,000
Secondary fluid	283	1228

Table 3
Geometrical parameters of the primary nozzle [22].

Geometrical parameters	Value
Diameter of nozzle inlet section	87.5 mm
Diameter of nozzle outlet section	52.5 mm
Diameter of nozzle throat	30 mm
Expand angle of nozzle	8°
Length of nozzle	231 mm

Table 4
Inlet flow conditions of the primary nozzle [22].

Working fluid	Temperature (K)	Pressure (Pa)
Primary fluid	390.15	87,000

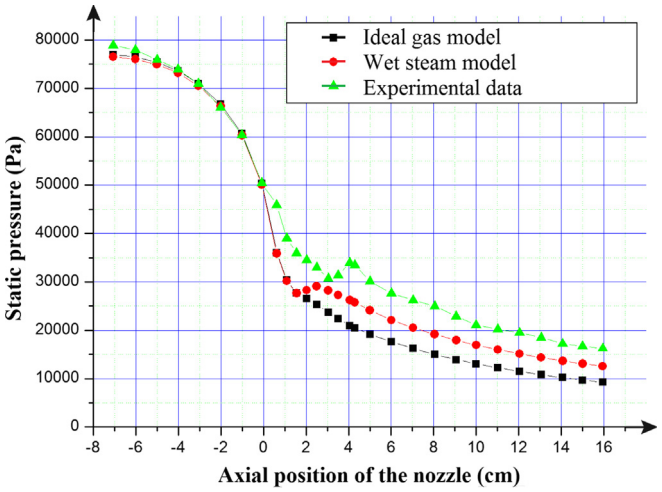

Fig. 5. Comparison of axial pressure distributions between two numerical methods and experimental data [22].

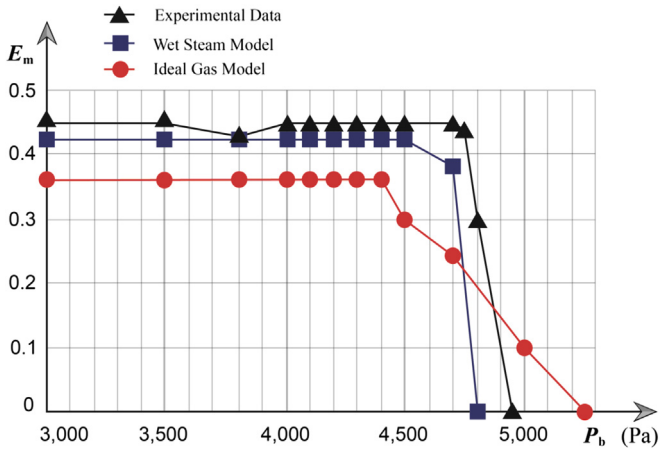

Fig. 6. Comparison of entrainment ratio between two numerical models with experimental data [19].

condensation in the steam ejector, five levels of superheated primary steam, 0 K, 10 K, 20 K, 30 K, and 40 K, were studied, and detailed results are provided in following sections.

4.2. The effect of primary steam superheating on the steam condensation in nozzle

The effects of the primary steam superheating on droplets nucleation rate along the nozzle axis is depicted in Fig. 7. The initial condensing occurrence position (Wilson point) happens downstream of the nozzle throat. For the primary steam without superheating, Wilson point occurs at $x = 2.9$ cm. Then, its occurrence is postponed to further downstream if the superheated level is increased. For the 40 K superheated primary steam, its Wilson point is found at $x = 3.1$ cm. Therefore, the increase of the primary steam superheating level can delay the occurrence of spontaneous condensation in nozzle.

The superheating influences on the droplet growth rate along the nozzle axis are depicted in Fig. 8. For the primary steam without superheating, its droplet growth rate peaks at 4000 microns/s at $x = 3$ cm. Then, the growth rate is considerably reduced and the

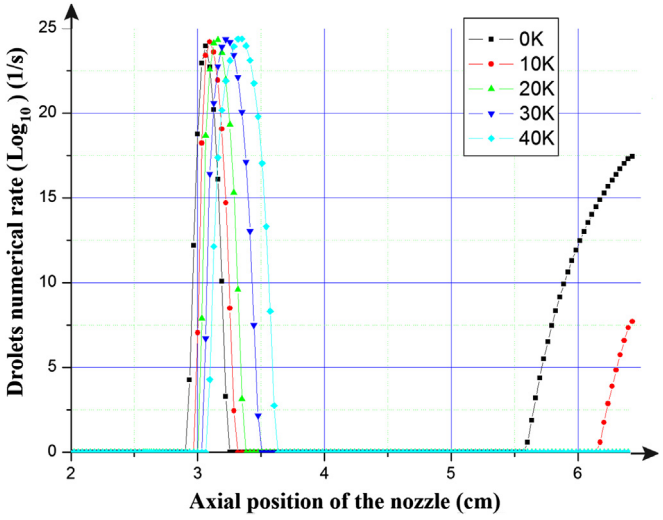

Fig. 7. Comparison of axial droplets nucleation rate with respect to different superheating treatments.

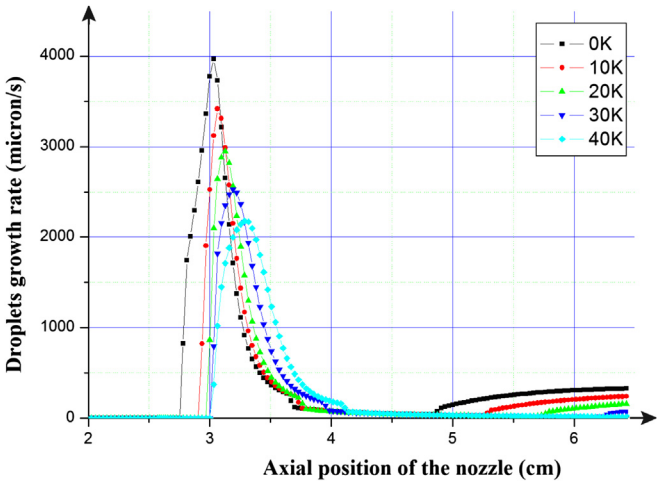

Fig. 8. Comparison of axial droplet growth rate with respect to different superheating treatments.

occurrence of the droplets peak growth rate is also postponed to further downstream if the superheated level is increased. For the 40 K superheated primary steam, its maximum droplet growth rate is 2100 microns/s at $x = 3.3$ cm. Consequently, the 40 K superheating leads to an almost 50% reduction in droplet growth rate during the spontaneous condensation.

The formed droplets average radius is also examined for different levels of superheating operation (Fig. 9). It is found that the droplets average radius is negatively related with steam superheated levels. For the primary steam without superheating, a maximum droplets average radius of 0.017 microns is formed. However, when the primary steam is superheated about 40 K, the largest averaged droplets radius is 0.010 microns, which means this superheating operation contributes a 40% droplets size refinement comparing with the original averaged droplets size.

4.3. The effect of primary steam superheating on the steam ejector performance

To assess the superheating operation influences on the steam ejector pumping performance, the entrainment ratio (E_m) with

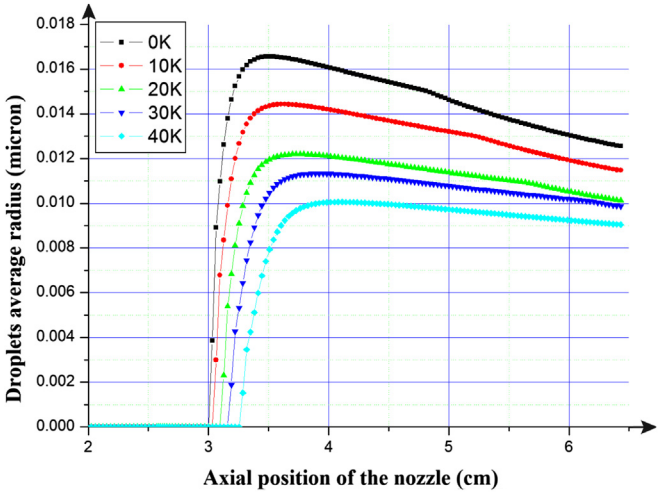

Fig. 9. Comparison of axial droplets average radius with respect to different superheating treatments.

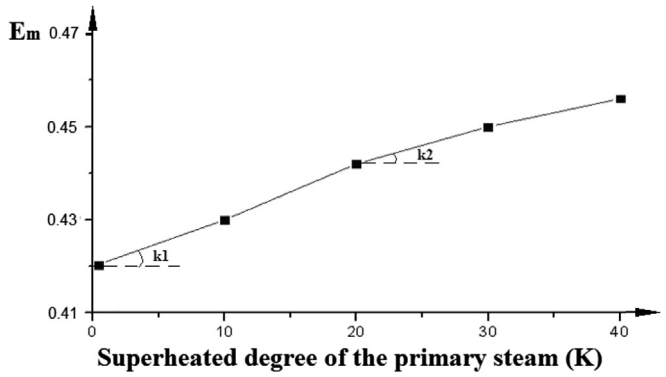

Fig. 10. Plot of entrainment ratio with respect to different superheated levels.

respect to different superheated levels is shown in Fig. 10. In general, the superheating operation promotes the entrainment ratio for all the studied cases. However, the E_m curve can be divided into two parts based on the averaged curve slopes. When the superheating operation of the primary steam is kept within 0 K–20 K, the E_m curve shows a slope of $k_1 = 0.001$. When the superheated level is maintained between 20 K–40 K, the slope of the E_m curve is decreased to $k_2 = 0.00075$. Therefore, the E_m growth rate due to the superheating effects slows down about 25% for 20 K–40 K superheated primary steam comparing with 0 K–20 K. This result indicates the E_m is not constantly increased with the primary steam superheating operations at the same growth rate. Taking the energy cost of generating superheated primary steam in to consideration, it might be not a good practical choice for the steam ejector to be operated with over 20 K superheated primary steam as it will require more energy input and only generate less E_m improvement as an output.

5. Conclusions

The spontaneous condensation need to be taken into account for steam ejector simulation, and it can further improve the entrainment ratio and critical back pressure prediction accuracy comparing with the simulation neglecting this phenomenon. The wet steam model being used in this study can capture the internal flow thermodynamics of the steam ejector and provide a close prediction of the ejector pumping performance.

The superheating operation of the primary steam can weaken the spontaneous condensation intensity and postpone its occurrence in the nozzle of the steam ejector. Due to the droplets nucleation refinement for the condensation of superheated steam, the mixing process between the primary and the secondary fluids is improved. Consequently, a higher entrainment ratio is achieved. However, the superheating operation may not exceed 20 K, as its contribution on entrainment ratio improvement is not as significant as 0 K–20 K superheating, and too much superheating will requires more energy as input, which is not a practical solution to further improve the steam ejector pumping performance.

Acknowledgment

The financial support provided by the Liaoning Natural Science Foundation (ID20102073), the Foundation of International Cooperation Project (ID7440015), the Doctoral Foundation for Returning-back Scholar of the China Ministry of Education (ID18504032) and the Australian Research Council (IDDP130100819) are gratefully acknowledged.

References

[1] Chunnanond K, Aphornratana S. An experimental investigation of a steam ejector refrigerator. Appl Therm Eng 2004;24:311–22.
[2] Huang BJ, Chang JM, Wang CP, Petrenko VA. A 1-D analysis of ejector performance. Int J Refrig 1999;22:354–64.
[3] Eames IW, Aphornratana S, Haider H. A theoretical and experimental study of a small-scale steam jet refrigerator. Int J Refrig 1995;18:378–86.
[4] Ouzzane M, Aidoun Z. Model development and numerical procedure for detailed ejector analysis and design. Appl Therm Eng 2003;23:2337–51.
[5] Bartosiewicz Y, Aidoun Z, Desevaux P, Mercadier Y. Numerical and experimental investigations on supersonic ejectors. Int J Heat Fluid Flow 2005;26:56–70.
[6] Desevaux P, Marynowski T, Khan M. CFD prediction of supersonic ejectors performance. Int J Turbo Jet Engines 2006;23:173–81.
[7] Varga S, Oliveira AC, Diaconu B. Numerical assessment of steam ejector efficiencies using CFD. Int J Refrig 2009;32(6):1203–11.
[8] Wang XD, Dong JL. Numerical study on the performances of steam-jet vacuum pump at different operating conditions. Vacuum 2010;84:1341–6.
[9] Dai XC, Huo J. Numerical simulation on flow structure of a steam-jet pump influenced by primary nozzle geometries. Appl Mech Mater 2012;130–134:1703–7.
[10] Wang XD, Dong JL, Wang T, Tu JY. Numerical analysis of spontaneously condensing phenomena in nozzle of steam-jet vacuum pump. Vacuum 2012;86(7):861–6.
[11] Wang XD, Lei HJ, Dong JL, Tu JY. The spontaneously condensing phenomena in a steam-jet pump and its influence on the numerical simulation accuracy. Int J Heat Mass Transfer 2012;55(17):4682–7.
[12] Sharifi N, Boroomand M, Kouhikamali R. Wet steam flow energy analysis within thermal-compressors. Energy 2012;47:609–19.
[13] Ludwing EE. Applied process design for chemical and petrochemical plants. 3rd ed., vol. 1. Butterworth-Heinemann; 1999.
[14] Ishazaki K, Ikohagi T, Daiguji HA. High-resolution numerical method for transonic non-equilibrium condensation flows through a steam turbine cascade. In: Proceedings of the 6th international symposium on computational fluid dynamics, vol. 1; 1995. p. 479–84. Lake Tahoe, Nevada.
[15] Young JB. An equation of state for steam for turbomachinery and other flow calculations. J Eng Gas Turbines Power 1988;110(1):1–7.
[16] Young JB. Two-dimensional, nonequilibrium, wet-steam calculations for nozzles and turbine cascades. J Turbo Mach 1992;114(7):569–79.
[17] Launder BE, Spalding DB. The numerical computation of turbulent flows. Comp Meth Appl Mech Eng 1974;3:269–89.
[18] Shih TH, Liou WW, Shabbir A, Yang Z, Zhu J. A new k–ε eddy-viscosity model for high Reynolds number turbulent flows – model development and validation. Comput Fluids 1995;24(3):227–38.
[19] Sriveerakul T, Aphornratana S, Chunnanond K. Performance prediction of steam ejector using computational fluid dynamics: part 1. Validation of the CFD results. Int J Therm Sci 2007;46:812–22.
[20] Pianthong K, Seehanam W, Behnia M, Sriveerakul T, Aphornratana S. Investigation and improvement of ejector refrigeration system using computational fluid dynamics technique. Energy Convers Manag 2007;48:2556–64.
[21] Kader B. Temperature and concentration profiles in fully turbulent boundary layers. Int J Heat Mass Transfer 1981;24(9):1541–4.
[22] Bakhtan F, Mohammadi Tochai MT. An investigation of two-dimensional flows of nucleating and wet steam by the time-marching method. Int J Heat Fluid Flow 1980;2(1):5–18.